Energy and exergy (2E) analysis of an optimized linear Fresnel reflector for a conceptual direct steam generation power plant

Eduardo González-Mora[1], Ma. Dolores Durán-García[1]

[1] Ingeniería en Sistemas Energéticos Sustentables. Facultad de Ingeniería, Universidad Autónoma del Estado de México, Toluca (México)

Abstract

Direct steam generation is a promising alternative to conventional HTF for solar thermal power plants. The optical equivalence of parabolic through collectors and linear Fresnel reflector demonstrated by several authors has led to the proposal of the integration of direct steam generation in linear Fresnel reflector systems for Steam Rankine power plants; as the Puerto Errado (Portugal), Kimberlina (USA) or Liddell (Australia). With this background, in the present paper a 2E analysis (energy and exergy) of a conceptual configuration solar power plant with Fresnel reflectors and direct steam generation, coupled to a Steam Rankine power cycle, is developed in order to establish a reference for a future implementation of this technology and show its viability against parabolic trough plants in México.

Keywords: LFR, DSG, Steam Rankine, energy, exergy

1. Introduction

Solar plants for conversion of thermal energy into electrical energy through power cycles have been oriented to solar fields with parabolic trough collectors (PTC). In recent years, there has been an increasing interest in using Fresnel reflectors due to low operating costs and the possibility of using direct steam generation. Unlike the parabolic collector, the analysis has been carried out by different research groups are oriented towards a single configuration of Fresnel reflectors (LFR), which still limits the analysis of results.

Commercially, direct steam generation (DSG) is still not in use because the PTC presents thermal stress problems. However, Fresnel reflectors do not present this disadvantage, so that currently one of the trends is towards this direction since it avoids the use of exchangers of heat and increases thermal performance by simplifying the configuration of the entire system. The DSG implies that the only working fluid is water, circulated through the solar field, where a phase change occurs. Then, the steam, at high pressure and temperature, is injected into the block. However, the technical limitations of using DSG in PTC that does not occur in the LFR, such as low thermal stresses, has made the tendency to perform power cycles with CSP and DSG using LFR, (Coco-Enríquez et al., 2013; Montes Pita, 2008; Ravelli et al., 2016).

Power plant modelling plays a crucial role in the design assessment and prediction of plant performance. This implies performing simulations to obtain background for future application. Aforementioned, it is essential to support the decisions related to the investment and design of CSP plants, since this helps in the prediction of the economic, energetic and operational characteristics of a real plant; outwardly the associated risks of possible accidents and system failures, which may render an installation unusable (Morin, 2012).

In this regard, several researchers have performed DSG analyzes with LFR, such as Giostri et al. (2013) compare the thermal performance of two solar plants (PTC with thermal oil and LFR with DSG) and show that the solar field using DSG presents better performance than if oil is used for the same operating conditions; Similarly, Sun et al. (2015) simulated numerically a solar plant with a parabolic channel in recirculation through a 2E analysis, to determine the energy and exergy efficiency of the system. Alternatively, Montes et al. (2016) have developed a thermal model applied to the comparative study of the thermal performance of the LFR receiver based on different parameters over the FRESDEMO field.

doi:10.18086/swc.2019.18.07 Available at http://proceedings.ises.org

In the present, a 2E analysis is developed for a configuration of a conceptual solar power plant with Fresnel reflectors and direct steam generation for Agua Prieta, Sonora; using an optically optimized LFR field. The developed model differs from those presented by other authors in the sense that the Adiutori methodology (2017) is introduced to avoid the use of the convective coefficient in a heat transfer study in solar concentration systems. Thus, the model reduces the calculation time and ensures a better tolerance of convergence in the results.

1.1. Structure and scope

As mentioned previously, a simple and flexible heat transfer model is developed, which will be described in detail in Section 3 taking into consideration de opto-geometric description presented in Section 2. Regarding the opto-geometric description, the Fresnel field has been optimized for the locality, so more energy can be used for the thermal process; while the 1-D thermohydraulic model has been developed (Alobaid, 2018), and validated with simulations done by another researchers over the FRESDEMO field (Mertins, 2009; Montes et al., 2016), in order to quantify the energy and exergy in the receiver and the whole system as, exploiting the geometrical properties of the model.

2. Opto geometric description of the LFR field

Even though the optical nature of LFRs is simple, there are very few data available to describe a Fresnel reflector field (Boito and Grena, 2016); many parameters need to be considered for the design of a Linear Fresnel Reflector Systems (Karathanasis, 2019). Considering some descriptions of various Fresnel reflectors, a field similar to the configuration of FRESDEMO (Fig. 1) is assumed to fix some design parameters; which is located at Plataforma Solar de Almería, Spain.

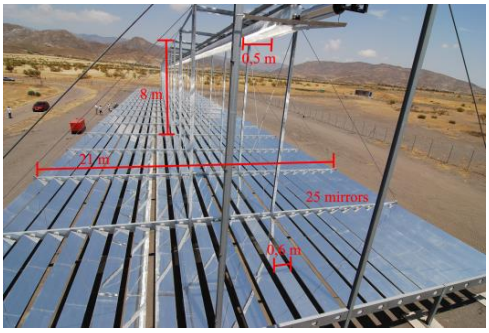

Fig. 1: Main geometrical parameters of the FRESDEMO field (Bernhard et al., 2014).

The conceptual solar power plant takes the FRESDEMO's field as reference, so an optical optimization has been done for the city of Agua Prieta, Sonora (North-West of México), which full description has been done for optimizing the intercept factor, result of having increased the height of the receiver and modified the CPC of the second stage of the cavity, maintaining the opening area of the receiver (González-Mora and Durán García, 2018).

In Tab. 1 the geometric description of the field is shown, while in Fig. 2 the IAM is shown and Fig. 3 the average optical concentration in the receiver plane. These graphs are used in the thermal model to establish the variance in output performance of a solar collector as the angle of the sun changes regarding the surface of the collector.

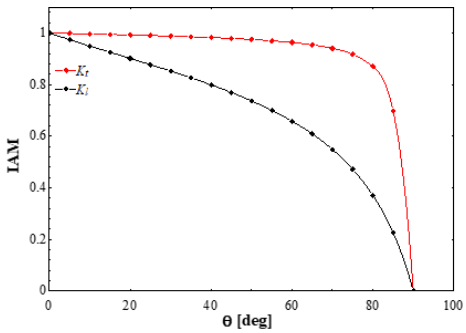

Fig. 2: Incidence angle modifiers for longitudinal (K_l) and transverse (K_t) directions (González-Mora and Durán García, 2018)

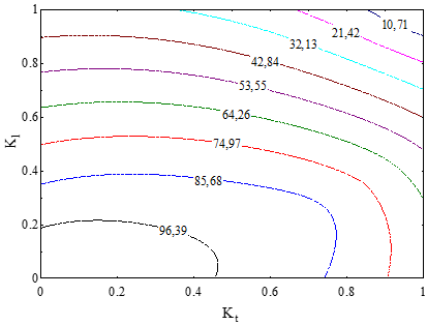

Fig. 3: Average optical concentration in the receiver plane

Tab. 1: Geometrical parameters of the optimized field for Agua Prieta, Sonora (González-Mora and Durán García, 2018).

Parameter	Agua Prieta
Number of primary mirrors	25
Solar field width $[m]$	21
Total length of the primary mirrors $[m]$	100
Width of the primary mirrors $[m]$	0,6
Filling factor	0,7143
Receiver height $[m]$	15
Receiver width $[m]$	0,5
Absorber tube outer diameter $[m]$	0,14
Absorber tube inner diameter $[m]$	0,125
Semi-angle acceptance of the CPC [°]	66,30
Intercept factor	0,7231
Receiver length $[m]$	100
Geometric concentration of the CPC	1,1368
Geometric concentration of the entire field	34,1046
Peak optical concentration	107,1430

3. Thermal model of the LFR

Taking as a starting point the models described by Montes et al. (2016), who applied the analysis for the FRESDEMO field, and the one from Veynandt (2011), who carried out the analysis of direct production of hot air Fresnel field, the 2E thermal model for the receiver is developed. The model proposed uses the energy balance equations at each surface of the cavity, schematically shown in Fig. 4 a. In Fig. 4 b the thermal resistance model equivalent to the heat transfer in the receiver cavity is represented. All the terms in Fig. 4 are defined in Tab. 2.

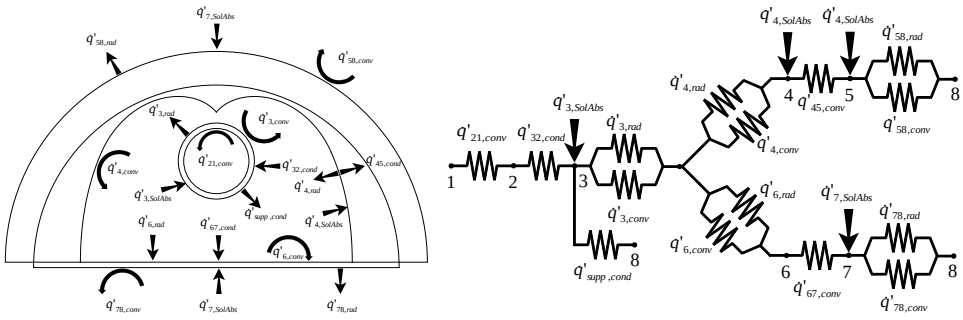

(a) Cross-section of the cavity in the receiver **(b) Thermal resistance model for the receiver cavity**

Fig. 4: Heat transfer model in the cavity.

The thermal energy equations are determined by applying the energy balance to each surface of the cross-section of the receiver cavity according to the resistant thermal model of the Fig. 4 (b); with eqs. (1) – (6) and an additional balance equation for the change in enthalpy of the HTF while flowing through the absorber tube, eq. 7.

$$\dot{q}'_{21,conv} = \dot{q}'_{32,cond} \quad \text{(eq. 1)}$$

$$\dot{q}'_{3,SolAbs} = \dot{q}'_{32,cond} + \dot{q}'_{3,rad} + \dot{q}'_{3,conv} + \dot{q}'_{supp,cond} \quad \text{(eq. 2)}$$

$$\dot{q}'_{45,cond} = \dot{q}'_{4,SolAbs} + \dot{q}'_{4,rad} + \dot{q}'_{4,conv} \quad \text{(eq. 3)}$$

$$\dot{q}'_{45,cond} = \dot{q}'_{58,rad} + \dot{q}'_{58,conv} \quad \text{(eq. 4)}$$

$$\dot{q}'_{67,cond} = \dot{q}'_{6,rad} + \dot{q}'_{6,conv} \quad \text{(eq. 5)}$$

$$\dot{q}'_{7,SolAbs} + \dot{q}'_{67,cond} = \dot{q}'_{78,rad} + \dot{q}'_{78,conv} \quad \text{(eq. 6)}$$

$$\dot{q}'_{21,conv} = \frac{\dot{m}}{L_{HCE}}(h_{1sal} - h_{1ent}) \quad \text{(eq. 7)}$$

The terms of conduction, convection, and radiation will be treated first as thermal resistance. The advantage of using the concept of thermal resistance lies in the ease of working with the three mechanisms of heat transfer together, so that heat transfer can be encompassed by:

$$\dot{q}' = \frac{\Delta T}{R'_{ter,tot}} \quad \text{(eq. 8)}$$

Tab. 2: Definition of heat flux in the cavity.

Heat flux $[W/m]$	**Heat transfer mode**	**Heat transfer path**	
		From	**To**
$\dot{q}'_{21,conv}$	Convection	Inner absorber tube	Heat transfer fluid
$\dot{q}'_{32,cond}$	Conduction	Outer absorber tube	Inner absorber tube
$\dot{q}'_{supp,cond}$	Conduction	Outer absorber tube	HCE supports
$\dot{q}'_{3,SolAbs}$	Absorption of solar radiation	Incident solar radiation	Outer absorber tube
$\dot{q}'_{3,rad}$	Radiation	Outer absorber tube	Cavity
$\dot{q}'_{3,conv}$	Convection	Outer absorber tube	Cavity
$\dot{q}'_{4,rad}$	Radiation	CPC surface	Cavity
$\dot{q}'_{4,conv}$	Convection	CPC surface	Cavity
$\dot{q}'_{4,SolAbs}$	Absorption of solar radiation	Incident solar radiation	CPC surface
$\dot{q}'_{45,cond}$	Conduction	CPC surface	Insulation
$\dot{q}'_{58,rad}$	Radiation	Insulation	Environment
$\dot{q}'_{58,conv}$	Convection	Insulation	Environment
$\dot{q}'_{6,rad}$	Radiation	Inner Pyrex surface	Cavity
$\dot{q}'_{6,conv}$	Convection	Inner Pyrex surface	Cavity
$\dot{q}'_{67,cond}$	Conduction	Inner Pyrex surface	Outer Pyrex surface
$\dot{q}'_{7,SolAbs}$	Absorption of solar radiation	Incident solar radiation	Outer Pyrex surface
$\dot{q}'_{78,rad}$	Radiation	Outer Pyrex surface	Environment
$\dot{q}'_{78,conv}$	Convection	Outer Pyrex surface	Environment

3.1. Convection heat transfer

To calculate the heat transfer by convection between the three internal surfaces of the cavity, there is no direct methodology, due to the geometry that involves the relationship between non-conventional surfaces; however,

using a series of dimensionless groups it is possible to apply it to a great variety of cases with relevant modifications (Alhama López, 2012; Simon et al., 2017). Some correction proposals have been made for the relationships of conventional surfaces through a complete and detailed study of the geometry of the CPC, the most relevant being the one proposed by Veynandt (2011) and Montes et al. (2016), who proposes to approximate the cavity to an annular space between two long concentric cylinders (where the inner cylinder, absorber, is warmer than the outside, free flow of the cavity), to use as an approximation the correlation of Raithby and Hollands (1975), leading to:

$$\dot{q}'_{conv,i} = \frac{(T_i - T_c)}{R'_{i,conv}} \quad \text{(eq. 9)}$$

where T_i is the temperature of the i-th surface (outer absorber tube, CPC or inner Pyrex surface), and T_c represents the corrected temperature of the weighted surface temperatures, which is based on a detailed study of the isothermal lines in the stratified temperature distribution for the cavity, validated by the experimental work and the numerical simulations of Kuehn and Goldstein (1976).

For the back shell of the insulation, the convective heat loss is calculated by different correlations for the case of wind or absence of wind; if the back shell of the insulation is considered as a horizontal semi-cylinder, the correlation of Churchill and Chu (1975) is applicable. In the case of forced convection, the correlation of Žukauskas (1972) is adequate; considering the external diameter of the absorber as the characteristic length of the system.

The glass window in the receiver is modelled as a horizontal plate heated by the bottom so that the convective heat loss is calculated by different correlations for the case of wind or absence of wind. If there is no presence of wind, the Nusselt number is determined by the McAdams correlation (1954); otherwise, the Pohlhausen relation is applicable in the case of laminar flow (1921); while, if one has a turbulent flow condition, the relationship of Chilton and Colburn is adequate (Bergman et al., 2011).

Internal convection from the inner tube to the HTF is divided into two zones (involving the three fluid regimes):

- Monophasic fluid (subcooled liquid and superheated steam).
- Two-phase fluid (liquid-vapour mixture).

In the first case, the Gnielinski correlation (Bergman et al., 2011) is used, which has the advantage that it is valid for a large interval of the Reynolds number. The relationship of Gnielinski is complemented with the friction factor described by Zigrang and Silvester (Nellis and Klein, 2009). In the second case, the correlation of Gungor and Winterton (1986) for two-phase flow is used because of its simplicity. One of the advantages of this model is that it can be used to predict the behaviour of any working fluid, both single-phase and two-phase.

3.2. Radiation heat transfer

The heat transfer by radiation $\dot{q}'_{ij,rad}$, is determined by the Stefan-Boltzmann equation for heat flux between two bodies with emittance ε_i and surface temperature T_i, considering that in the case of a small convex object - like the receiver - this thermal energy radiates towards a much larger surface (the equivalent sky) (Bejan, 1993; Duffie and Beckman, 2013; Nellis and Klein, 2009), as stated in eq. 10.

$$\dot{q}'_{ij,rad} = \frac{T_i - T_j}{R'_{ij,rad}} \quad \text{(eq. 10)}$$

To model the transfer of heat by radiation from one surface to another inside the cavity, as in the case of the absorber tube to the window of the receiver, the use of thermal resistance will not be used; so that the equation modelling this phenomenon considers the radiosity and the vision factor of the system only as a surface phenomenon. According to Siegel and Howell (Howell et al., 2015), the radiosity can be determined by

$$J_i = \varepsilon_i \sigma T_i^4 + (1 - \varepsilon_i) \sum_j J_j F_{i-j} \quad \text{(eq. 11)}$$

where J_i is the radiosity of the surface, ε_i is the emittance, T_i is the temperature of the surface and F_{i-j} is the surface vision factor from i to j, which is calculated using the eq. 10; that relates the geometries of the surfaces involved in the process, as well as the areas of each surface (Howell et al., 2015).

$$F_{i-j} = \frac{1}{A_i} \int_{Ai} \int_{A_j} \frac{\cos\theta_i \cos\theta_j}{\pi S^2} dA_j dA_i \quad \text{(eq. 12)}$$

where S is the normal distance between surfaces, θ is the angle of the normal to the surface and A is the area of the surface. It is necessary to emphasize that the normal of the surface i points towards the surface j, and that the surface j points towards the surface i. In the case of closed cavities, the sum of the vision factors must be unitary (Howell et al., 2015). Thus, the heat transfer by radiation (per unit length) for each surface is then determined by

$$\dot{q}'_{i,rad} = L_i\left(\varepsilon_i \sigma T_i^4 + (1-\varepsilon_i)\sum_j J_j F_{i-j}\right) \quad \text{(eq. 13)}$$

3.3. Conduction heat transfer

The conduction heat transfer is modelled according to eq. 14.

$$\dot{q}'_{ij,cond} = \frac{T_i - T_j}{R'_{ij,cond}} \quad \text{(eq. 14)}$$

The heat losses of the supports are determined by considering that each HCE is placed in the focal line of the concentrator through supports that go from the structure of the concentrator to the absorber. There is a support at the end of each HCE, 17 in $100\ m$ (approximately every $6\ m$ of the receiver length). The losses of the support are approximated by treating the support as an infinite fin with a base temperature of $10\ K$ less than the temperature of the external surface of the absorber (T_3) at the point where the support is fixed. This estimated base temperature accounts for heat losses along the short distance from the support fixation to the minimum area of the cross-section, which is assumed to be the base of the fin ($\sim 5\ cm$ with $\sim 4\ cm$ insulation) (Forristall, 2003; Montes et al., 2016). The thermal resistance and the heat loss of the support are estimated with the following equations (Bergman et al., 2011):

$$R'_{supp,cond} = \frac{L_{HCE}}{\sqrt{\left(\overline{h}_c P_b k A_{cs}\right)_{c,supp}}} \quad \text{(eq. 15)}$$

$$\dot{q}'_{supp,cond} = \frac{T_{supp} - T_8}{R'_{supp,cond}} \quad \text{(eq. 16)}$$

where $\overline{h}_c$ is the average support convection coefficient, P_b is the support perimeter, k is the thermal conductivity of the support, A_{cs} is the minimum cross-sectional area of support. The coefficient $\overline{h}_c$ depends on the wind speed. In the case that there is no wind, Churchill and Chu's relationship (1975) allows Nusselt's number to be determined. In the case of wind, the Churchill and Bernstein (1977) relationship is applicable. The reference temperature for calculations is estimated by $(T_{base} + T_6)\ /\ 3$ as proposed by Forristal (2003). In this model, the heat losses in the tubes manifold are ignored.

3.4. Absorption of solar radiation

The absorption of solar radiation in the tube, the CPC and the window are considered as surface phenomena, so each term can be calculated by eqs. 17-19, where τ_{67} is the Pyrex glass transmittance, ρ_4 is the CPC reflectance, α_{ij} is the absorptance for the tube, CPC and Pyrex glass, and $\dot{q}'_{in,rec-HCE}$ is the incident solar radiation flux in the receiver, taking into account the primary mirror's reflectance and the IAM.

$$\dot{q}'_{3,SolAbs} = \tau_{67}\rho_4\alpha_{23}\dot{q}'_{in,rec-HCE} \quad \text{(eq. 17)}$$

$$\dot{q}'_{4,SolAbs} = \tau_{67}\alpha_{45}\dot{q}'_{in,rec-HCE} \quad \text{(eq. 18)}$$

$$\dot{q}'_{7,SolAbs} = \alpha_{67}\dot{q}'_{in,rec-HCE} \quad \text{(eq. 19)}$$

3.5. Energy efficiency

The thermal efficiency of the first law is defined as the quotient of the useful power and the available power (or input to the system). Thus, the thermal efficiency of the Fresnel reflector is calculated using eq. 20, and the receiver efficiency with eq. 21.

$$\eta_{I,LFR} = \frac{\dot{Q}_{HTF}}{\dot{Q}_{in,pm}} \quad \text{(eq. 20)}$$

$$\eta_{I,rec} = \frac{\dot{Q}_{HTF}}{\dot{Q}_{in,rec}} \quad \text{(eq. 21)}$$

3.6. Exergy analysis

The input exergy to the system is the exergy irradiated from the Sun. The Parrot's model (1978) quantifies the

exergy of solar radiation on the earth's surface; that is, consider the transfer of radiative exergy between the surface of the Sun and the earth's surface, as stated in eq. 22.

$$\dot{B}_b = DNI\left[1 - \frac{4}{3}\frac{T_0}{T_s}(1 - cos\,\theta_s)^{\frac{1}{4}} + \frac{1}{3}\left(\frac{T_0}{T_s}\right)^4\right] \quad \text{(eq. 22)}$$

Considering a steady-state system is, the exergy balance of the receiver will be:

$$\dot{B}_{rec} = \left(1 - \frac{T_0}{T_3}\right)\dot{Q}_{in,rec} \quad \text{(eq. 23)}$$

3.7. Exergy efficiency

Similarly to the energy efficiency, the exergy efficiency is calculated for the Fresnel reflector (eq. 24) and for the receiver (eq. 25).

$$\eta_{II,LFR} = \frac{\dot{B}_{rec}}{\dot{B}_b} \quad \text{(eq. 24)}$$

$$\eta_{II,rec} = \frac{\dot{B}_{HTF}}{\dot{B}_{rec}} \quad \text{(eq. 25)}$$

4. Thermal model validation

As explained in the previous section, the thermal model consists of 29 equations and 29 unknowns that are grouped into 7 final equations, eqs.1-7, which involve 7 well-defined groups:

- Group 1: 4 solar absorptive equations to calculate $\dot{q}'_{3,SolAbs}, \dot{q}'_{4,SolAbs}, \dot{q}'_{5,SolAbs}, \dot{q}'_{7,SolAbs}$)
- Group 2: 4 conduction equations ($\dot{q}'_{32,cond}, \dot{q}'_{supp,cond}, \dot{q}'_{45,cond}, \dot{q}'_{67,cond}$)
- Group 3: 6 convection equations ($\dot{q}'_{21,conv}, \dot{q}'_{3,conv}, \dot{q}'_{4,conv}, \dot{q}'_{58,conv}, \dot{q}'_{6,conv}, \dot{q}'_{78,conv}$)
- Group 4: 5 radiation equations ($\dot{q}'_{3,rad}, \dot{q}'_{4,rad}, \dot{q}'_{58,rad}, \dot{q}'_{6,rad}, \dot{q}'_{78,rad}$)
- Group 5: 3 radiosity equations
- Group 6: 7 balances, one per node from 2 to 7 plus the central one of the cavity
- Group 7: fluid energy balance to calculate the increase in the enthalpy of the fluid

At this point, it is pertinent to mention that the proposed model is non-linear, however the methodology proposed by Adiutori (2017) is used with the purpose of being able to solve directly for temperatures and heat fluxes, transforming the convective coefficients by functional relations of the heat flow and temperatures, thus avoiding the solution by iterative methods, as proposed by Heimsath et al. (2013), although this does not exclude that the solution is numerical applied to each HCE of $5{,}88\ m$. This length has been chosen since 17 supports are distributed over $100\ m$ of length.

To validate the model, the analysis parameters of the Montes et al. (2016) model have been tested and the system of equations has been solved to obtain the temperatures and heat fluxes involved in the receiver. Once the analysis has been carried out, the results are compared with those shown by Montes Pita et al. (2016) and Mertins (2009) over the FRESDEMO field. The validation criterion proposed is that for the reported graphs of heat losses, the following conditions must be met:

- Heat losses must be of the same order of magnitude (400 to $1800\ W/m$)
- The graph must be congruent with both models
- There should not be a discrepancy greater than 10%

The first two conditions are directly evaluated when comparing the data of the overlaid graphs in Fig.5. where it is appreciated that the results are bounded by both models. The third condition is verified with the error bars shown in Fig. 6 (a) and (b) where it is perceived that the most significant error is at the beginning of the heating zone, although it does not exceed a value of more than 5%, therefore, the value of the discrepancy in this zone is accepted.

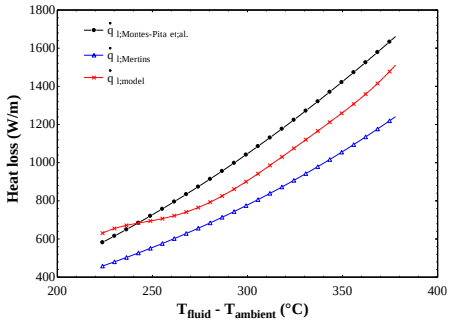

Fig. 5: Comparison between the thermal losses calculated by the thermal model of Montes et al. (2016); Mertins (2009) and proposed.

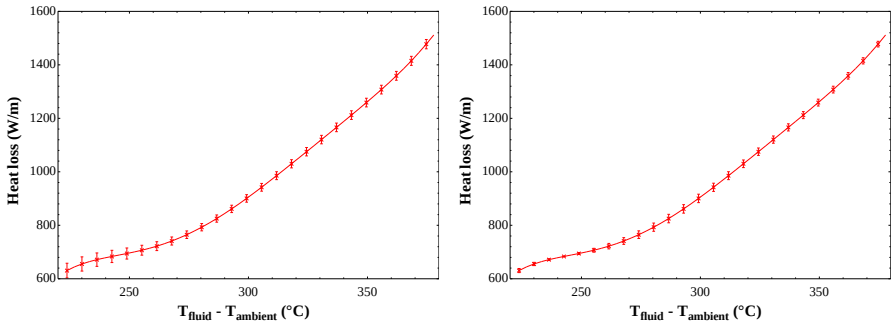

(a) Comparison with the Mertins model **(b) Comparison with the Montes et al. model**

Fig. 6: Error bars between models.

5. Thermal performance characterization of the system

Once the thermal model has been validated, we proceed to apply it directly to the case study with the objective of establishing the length of the loops that will make up the solar field; and also, to be able to thermally characterize the loop by means of an evaluation of the energy and exergetic performance to compare it with the performance of other Fresnel loops and even with parabolic channels for the same power range.

With the help of software Meteonorm (2018), it is possible to establish the climatological conditions that will be the initial values to begin the application of the model, which are summarized in the Tab. 3 for the design day, (June 21st).

The thermal model is applied to the simulation of each HCE that makes up the solar field that is described in Section 2, operating in steady-state in a single operation: preheating, evaporation and superheating. The optimized LFR field will heat 4,2 kg/s of steam at 100 bar enters at 518,3 K and leaving the field at 673,15 K, which are similar values with those adopted in other simulations (Coco Enríquez et al., 2014; Montes et al., 2016).

Tab. 3: Meteorological data for Agua Prieta, Sonora

Parameter	21st June
Day of the year	172
Atmospheric pressure $[bar]$	0,886
Ambient temperature $[K]$	300,05
Effective sky temperature $[K]$	271,95
DNI $[W/m^2]$	856,4815
Wind speed $[m/s]$	4,1

The graph plotted in Fig. 7, shows the rise of temperature of water while flowing through the 623,5 m of the loop.

The length of the loop is divided into three regions:

- Preheating: 88,6 m (14,2%)
- Evaporation: 423,9 m (68%)
- Superheating: 111 m (17,8%)

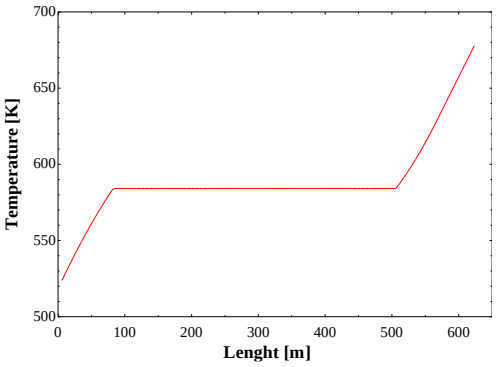

Fig. 7: Water/steam temperature along the optimized Fresnel loop in once-through operation mode.

The graph in Fig. 8 shows the increase in heat losses per unit length concerning the temperature difference between the fluid and the environment. When performing the thermal performance analysis of both the receiver (red line) and the concentrator (black line), it is clear that after the phase change, the decrease in performance is considerable. In the first HCE, the performance of the concentrator is 0,47 while that of the receiver is 0,71; at the exit of the loop, the first fall to 0,28 and the second to 0,42. This decrease in energy efficiency is shown in Fig.8.

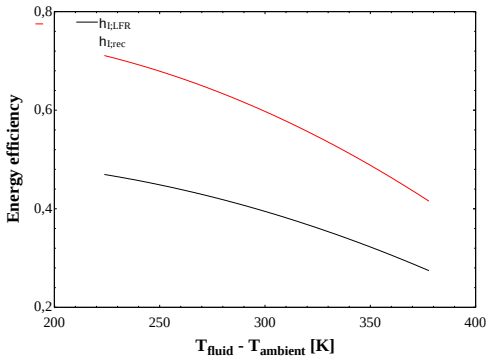

Fig. 8: Energetic performance of the linear Fresnel reflector and receiver.

Unlike energy efficiency, the exergetic performance of the receiver, it has different behaviour on the receiver's energy performance, but not the exergetic performance of the concentrator, as shown in Fig. 9. The above is explained because the energy efficiency decreases with increasing working temperature, since the heat loss is greater, while the exergy performance increases with temperature, but this increase is lower at higher temperatures. In the first HCE, the exergetic performance of the concentrator is 0,67 while that of the receiver is 0,14; at the exit of the loop, the first fall to 0,19 and the second reaches 0,40.

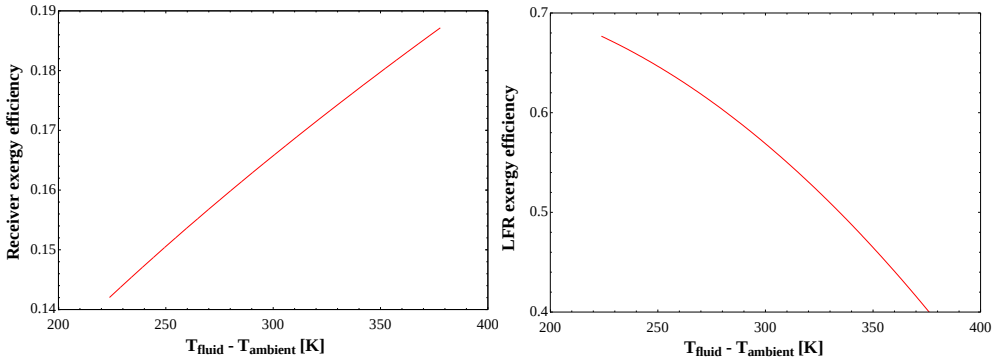

(a) **(b)**

Fig. 9: Exergetic performance. (a) Receiver and (b) of the linear Fresnel reflector.

6. Conclusions

The model to analyze the thermohydraulic behaviour is described, taking as reference models of heat transfer reported for Fresnel systems for direct steam generation. The pertinent parameters were adjusted to achieve the convergence, which was validated with error bars on the graphs of heat losses against the temperature difference of the fluid of work and the environment, reported by the mismatch models, where the error does not exceed 5% for the values reported by other researchers over the FRESDEMO field, in such a way that the adaptation of the model using the Adiutori's methodology for heat transfer is considered valid.

The difference with other models lies in two fundamental features: First, the model is implemented each $5{,}88\ m$, to simplify the simulation of losses through the supports. Second, the model is solved by a direct numerical method, in which all convection heat transfer equations are transformed into functions depending only on the temperature of each surface. This grants to solve the model directly for temperatures and heat flows with no iterative process.

Once the model has been validated with the FRESDEMO's simulations data, it has been applied to the locality of Agua Prieta, Sonora, in order to determine the length of the loop for a direct steam generation power plant, resulting in $623{,}5\ m$ with water/steam as the working fluid; where the optical optimization described in (González-Mora and Durán García, 2018), is appropriate to reduce the length of $1000\ m$ of the FRESDEMO field for the same thermal process.

7. Acknowledgements

The authors gratefully thank Dr Antonio Rovira (UNED), Prof. Eugene Adiutori (Ventuno Press) and Dr Alejandro Loza-Yáñez (UAEMex) who provided insight and expertise that greatly assisted the model. Although they may not agree with all the interpretations of this paper, any errors are our own and should not tarnish the reputations of these esteemed persons.

8. References

Adiutori, E., 2017. The new engineering, 3rd ed. Ventuno Press, Florida.

Alhama López, F., 2012. Análisis dimensional discriminado en mecánica de fluidos y transferencia de calor, 1st ed. Reverté.

Alobaid, F., 2018. Numerical Simulation for Next Generation Thermal Power Plants, Springer Tracts in Mechanical Engineering. Springer International Publishing.

Bejan, A., 1993. Heat transfer. John Wiley & Sons, Inc.

Bergman, T.L., Lavine, A.S., Incropera, F.P., Dewitt, D.P., 2011. Fundamentals of Heat and Mass Transfer, 7th ed. John Wiley & Sons, Inc.

Bernhard, R., Laabs, H.-J., de LaLaing, J., Eickhoff, M., 2014. Linear Fresnel Collector Demonstration on the PSA, Part I – Design, Construction and Quality Control. SolarPaces 1–10.

Boito, P., Grena, R., 2016. Optimization of the geometry of Fresnel linear collectors. Sol. Energy 135, 479–486. https://doi.org/https://doi.org/10.1016/j.solener.2016.05.060

Churchill, S.W., Bernstein, M., 1977. A Correlating Equation for Forced Convection From Gases and Liquids to a Circular Cylinder in Crossflow. J. Heat Transfer 99, 300–306.

Churchill, S.W., Chu, H.H.S., 1975. Correlating equations for laminar and turbulent free convection from a horizontal cylinder. Int. J. Heat Mass Transf. 18, 1049–1053. https://doi.org/10.1016/0017-9310(75)90222-7

Coco-Enríquez, L., Muñoz-Antón, J., Martínez-Val, J.M., 2013. Innovations on direct steam generation in linear Fresnel collectors. SolarPACES2013 00, 45721.

Coco Enríquez, L., Muñoz-Antón, J., Martínez-Val, J.M., 2014. Supercritical Steam power cycle for Line-Focus Solar Power Plants Supercritical Steam power cycle for Line-Focus Solar Power Plants, in: Nuclear and Renewable Resources International Conference. pp. 2–8. https://doi.org/10.13140/2.1.4031.7769

Duffie, J.A., Beckman, W.A., 2013. Solar Engineering of Thermal Processes, 4th ed. John Wiley & Sons, Inc.

Forristall, R., 2003. Heat Transfer Analysis and Modeling of a Parabolic Trough Solar Receiver Implemented in Engineering Equation Solver. Colorado.

Giostri, A., Binotti, M., Silva, P., Macchi, E., Manzolini, G., 2013. Comparison of Two Linear Collectors in Solar Thermal Plants: Parabolic Trough Versus Fresnel. J. Sol. Energy Eng. 135, 011001. https://doi.org/10.1115/1.4006792

González-Mora, E., Durán García, M.D., 2018. Optimización óptica de un reflector Fresnel lineal para generación directa de vapor, in: XLII SEMANA NACIONAL DE ENERGIA SOLAR. México.

Gungor, K.E., Winterton, R.H.S., 1986. A general correlation for flow boiling in tubes and annuli. Int. J. Heat Mass Transf. 29, 351–358. https://doi.org/10.1016/0017-9310(86)90205-X

Heimsath, A., Cuevas, F., Hofer, A., Nitz, P., Platzer, W.J., 2013. Linear Fresnel Collector receiver: Heat loss and temperatures. Energy Procedia 49, 386–397. https://doi.org/10.1016/j.egypro.2014.03.042

Howell, J.R., Menguc, M.P., Siegel, R., 2015. Thermal Radiation Heat Transfer, 6th ed. CRC Press, Boca Raton. https://doi.org/10.1115/1.3449647

Karathanasis, S., 2019. Linear Fresnel Reflector Systems for Solar Radiation Concentration: Theoretical Analysis, Mathematical Formulation and Parameters' Computation Using MATLAB. SPRINGER NATURE.

Kuehn, T.H., Goldstein, R.J., 1976. An experimental and theoretical study of natural convection in the annulus between horizontal concentric cylinders. J. Fluid Mech. 74, 695. https://doi.org/10.1017/S0022112076002012

McAdams, W.H., 1954. Heat Transmission, McGraw-Hill series in chemical engineering. McGraw-Hill.

Mertins, M., 2009. Technische und wirtschaftliche Analyse von horizontalen Fresnel-Kollektoren.

Meteonorm, 2018. Meteonorm.

Montes, M.J., Barbero, R., Abbas, R., Rovira, A., 2016. Performance model and thermal comparison of different alternatives for the Fresnel single-tube receiver. Appl. Therm. Eng. 104, 162–175. https://doi.org/10.1016/j.applthermaleng.2016.05.015

Montes Pita, M.J., 2008. Análisis Y Propuestas De Sistemas Solares De Alta Exergía Que Emplean Agua Como Fluido Calorífero. Universidad Politécnica de Madrid.

Morin, G., 2012. 16 – Optimisation of concentrating solar power (CSP) plant designs through integrated techno-economic modelling, in: Lovegrove, K., Stein, W. (Eds.), Concentrating Solar Power Technology. Elsevier, pp. 495–535. https://doi.org/10.1533/9780857096173.3.495

Nellis, G., Klein, S., 2009. Heat Transfer, Heat Transfer. Cambridge University Press.

Parrott, J.E., 1978. Theoretical upper limit to the conversion efficiency of solar energy 21, 227–229.

Pohlhausen, E., 1921. Der Wärmeaustausch zwischen festen Körpern und Flüssigkeiten mit kleiner reibung und kleiner Wärmeleitung. ZAMM - J. Appl. Math. Mech. / Zeitschrift für Angew. Math. und Mech. 1, 115–121. https://doi.org/10.1002/zamm.19210010205

Raithby, G.D., Hollands, K.G.T., 1975. A General Method of Obtaining Approximate Solutions to Laminar and Turbulent Free Convection Problems. Adv. Heat Transf. 11, 265–315. https://doi.org/10.1016/S0065-

2717(08)70076-5

Ravelli, S., Franchini, G., Perdichizzi, A., Rinaldi, S., Valcarenghi, V.E., 2016. Modeling of Direct Steam Generation in Concentrating Solar Power Plants. Energy Procedia 101, 464–471. https://doi.org/10.1016/j.egypro.2016.11.059

Simon, V., Weigand, B., Gomaa, H., 2017. Dimensional Analysis for Engineers, Mathematical Engineering. Springer International Publishing.

Sun, J., Liu, Q., Hong, H., 2015. Numerical study of parabolic-trough direct steam generation loop in recirculation mode: Characteristics, performance and general operation strategy. Energy Convers. Manag. 96, 287–302. https://doi.org/10.1016/j.enconman.2015.02.080

Veynandt, F., 2011. Cogénération héliothermodynamique avec concentrateur linéaire de Fresnel : modélisation de l'ensemble du procédé. Université de Tolouse.

Žukauskas, A., 1972. Heat Transfer from Tubes in Crossflow. Adv. Heat Transf. 8, 93–160. https://doi.org/10.1016/S0065-2717(08)70038-8